Locally defined quantum emission from epitaxial few-layer tungsten diselenide

Authors

Wei Wu,[1] Chandriker K. Dass,[2,3] Joshua R. Hendrickson,[2] Raul D. Montaño,[1,4] Robert E. Fischer,[5] Xiaotian Zhang,[6] Tanushree H. Choudhury,[6] Joan M. Redwing,[6,7] Yongqiang Wang,[8,9] and Michael T. Pettes[1,9,a]

Affiliations

[1] Department of Mechanical Engineering and Institute of Materials Science, University of Connecticut, Storrs, Connecticut 06269, USA.

[2] Air Force Research Laboratory, Sensors Directorate, Wright-Patterson Air Force Base, Ohio 45433, USA.

[3] KBRwyle, Dayton, OH, 45431, USA

[4] Department of Aerospace and Mechanical Engineering, University of Arizona, Tucson, Arizona 85721, USA.

[5] Center for Advanced Materials Characterization in Oregon (CAMCOR), University of Oregon, Eugene, Oregon 97403, USA.

[6] Department of Materials Science and Engineering, The Pennsylvania State University, University Park, Pennsylvania 16802, USA.

[7] 2D Crystal Consortium–Materials Innovation Platform, Materials Research Institute, The Pennsylvania State University, University Park, Pennsylvania 16802, USA.

[8] Materials Science and Technology Division, Los Alamos National Laboratory, Los Alamos, New Mexico 87545, United States

[9] Center for Integrated Nanotechnologies, Materials Physics and Applications Division, Los Alamos National Laboratory, Los Alamos, New Mexico 87545, USA.

[*] Author to whom correspondence should be addressed. pettesmt@lanl.gov

Abstract

Recently, single photons have been observed emanating from point defects in two-dimensional (2D) materials including WSe_2, WS_2, hexagonal-BN, and GaSe, with energy residing in the direct electronic band gap. Here, we report single photon emission from a nominally weakly emitting indirect band gap 2D material through deterministic strain induced localization. A method is demonstrated to create highly spatially localized and spectrally well-separated defect emission sites in the 750–800 nm regime in a continuous epitaxial film of few-layer WSe_2 synthesized by a multi-step diffusion-mediated gas source chemical vapor deposition technique. To separate the effects of mechanical strain from substrate or dielectric-environment induced changes in the electronic structure, we created arrays of large isotropically etched ultra-sharp silicon dioxide tips with spatial dimensions on the order of 10 μm. We use bending based on the small radius of these tips – on the order of 4 nm – to impart electronic localization effects through morphology alone as the WSe_2 film experiences a uniform SiO_2 dielectric environment in the device geometry chosen for this investigation. When the continuous WSe_2 film was transferred onto an array of SiO_2 tips, an ~87% yield of localized emission sites on the tips was observed. The outcomes of this report provide fundamental guidelines for integration of beyond-lab-scale quantum materials into photonic device architectures for all-optical quantum information applications.

Text

Single photon generation is a requirement for quantum key distribution and all-optical quantum computing and crucial for the advancement of quantum information technologies[1-6]. Beginning with WSe_2 in 2015[7], several recent studies have observed single photons originating from defect structures in two-dimensional (2D) materials such as mechanically exfoliated WSe_2[8-18], WS_2[14, 15],

1

hexagonal-BN[19], and GaSe[20, 21], and in chemical vapor deposition synthesized WSe$_2$[7] and hexagonal-BN[22] where second order photon correlation parameters have reached as low as 0.07–0.39 (Table S1, supplementary material). Optical emission energy in these systems resides within the electronic band gap and excitation had been provided by optical pumping[8-11, 14-16, 18, 20-22], and electrical charge injection[14]. Previous studies have postulated that non-uniform strain fields govern quantum emission in these materials[15, 16, 23] which may benefit secure communication technologies as the use of single photon sources requires both spatial control of the emission site and no more than one emitter per site[24-26]. However, the mechanism responsible for recent spatial control based on dielectrically non-uniform tent-pole style pillars[15, 16] remains unclear, as does the generality of conclusions based on these studies. Additionally, scalability also currently limits progress: lab-scale mechanical exfoliation and powder vapor transport growth of small crystallites constitute the only cases where this effect has been observed in semiconducting 2D materials[7-16, 20, 21].

Here, we demonstrate a method to create highly spatially localized and well-separated defect emission sites in a continuous film of few-layer epitaxial WSe$_2$ synthesized by a multi-step diffusion-mediated gas source chemical vapor deposition (CVD) technique[27]. The synthesis method employs W(CO)$_6$ and H$_2$Se vapor-phase sources enabling control over WSe$_2$ nucleation density and lateral domain growth which are necessary to achieve uniform epitaxial films on sapphire (0001). When the coalesced epitaxial WSe$_2$ film was transferred onto an array of ultra-sharp SiO$_2$ tips, we observed one order of magnitude longer bound exciton lifetimes from the tip apex compared to defect emission intrinsic to the film, where both defect types emitted in the ~725–810 nm wavelength regime. Narrow linewidth emission was seen arising from 13 out of 15 tips, and we present detailed analysis power, temperature, and quantum emission characterization

of one tip. Single photon generation at the tip apex was confirmed, where single photon purity reached ~70% at 3.8 K.

Uniaxial and biaxial tensile (compressive) strain reduces (increases) the electronic band gap in 2D transition metal dichalcogenide (TMD) materials such as MoS_2[28-31] and WSe_2[31-33]. This may lead to a quantum dot-type energy landscape if strain is applied locally and has been hypothesized to be the mechanism responsible for quantum emission from WSe_2 and WS_2 transferred onto tent pole-style engineered substrates[12, 15, 16] or patterned surfaces[13]. To separate the effects of mechanical strain from substrate- and/or dielectric-environment induced changes in the local electronic structure, we have created arrays of silicon dioxide tips with well-defined tip radii. Large 20 μm × 20 μm sputtered chromium pads were used as the hard mask while buffered oxide etchant was used to isotropically etch the tips from a ~10 μm-thick CVD SiO_2 film deposited onto sub-stoichiometric silicon nitride which acted as a dielectric etch stop. At the top (bottom) surfaces of the WSe_2 film, the tensile (compressive) strain can be estimated as

$$\varepsilon = h/(2r) \qquad (1)$$

where h is the thickness of the WSe_2 film and r is the tip radius. Figure 1 illustrates that by applying equation 1 to an $n = 1$–5 layer WSe_2 film with layer thicknesses of 6.491 Å[34] placed onto a 10-nm radius tip, a maximum strain of 3.2–16.2 % will arise at the film surface with a strain gradient on the order of 10^{10} %m^{-1} perpendicular to the film. This symmetric strain profile thus should have an observable effect on excitonic emission[33] and lifetime[35], although the true strain experienced will depend on a number of other issues such as compliance and adhesion energy. We note that a recent study[36] found an order of magnitude increase in the thermal expansion coefficient (α) of

several monolayer TMD materials compared to the bulk material. The relationship between α and elastic modulus (E) can be expressed as[37]:

$$\alpha \propto \gamma \rho c_v / E, \tag{2}$$

where γ is the Grüneisen parameter, ρ is the mass density, and c_v is the specific heat. Since α is inversely proportional to E, it is likely that mono- and few-layer TMD materials are significantly more compliant than their bulk counterparts and thus more able to be strained by the sharp tips in this work.

We make use of a recently developed vertical cold-wall CVD reaction scheme[27] to deposit WSe_2 over a roughly 1 cm^2 sapphire c-plane (0001) substrate, where prior challenges in wafer-scale synthesis have been solved by using H_2Se as the selenium precursor with a significant amount of excess chalcogen to obtain epitaxial films (Figures S1 and S2, supplementary material). Using an aberration-corrected transmission electron microscope (TEM), we estimate the film thickness was on the order of 5–15 layers. The epitaxial WSe_2 was then transferred onto the tips using a wet transfer technique (see supplementary material for additional details).

In order to determine the underlying carrier relaxation dynamics and single photon generation characteristics of the WSe_2, ultra-fast optical characterization was performed using a Ti:Sapphire femtosecond laser for time resolved photoluminescence (TRPL) and Hanbury Brown-Twiss (HBT) interferometry was performed using a HeNe continuous wave laser with spectral windows defined by inserting band-pass and tunable long- and short-pass filters into the beam path. A diagram of the beam paths for both experiments is given in Figure S3, supplementary material. Figures 2 S4, supplementary material, give the spectroscopic characterization results of optical emission arising from WSe_2 on the apex of an ultra-sharp SiO_2 tip. Additional comparison of the

emission spectra from the unstrained material and from the strained material at the tip apex, along with representative PL from non-quenching tip emitters is given in Figure 3 and Figure S5, supplementary material, where the free exciton emission at the tip apex exhibits a blue shift of 22.1±3.4 nm (47.3±8.3 meV) compared to the unstrained free exciton emission peaks. This is 1.2–8.5 times larger than observed for tent-pole-based studies[15, 16], although we note that since the elastic deformation is tensile at the upper WSe_2 surface and compressive at the lower surface, quantitative deconvolution of the strain-dependent emission spectra as per ref. [33] is not trivial. Our gas source CVD WSe_2 films contain grains smaller than the 0.7–1 μm excitation beam diameter, thus the contribution of grain boundary defects to quantum emission is an additional remaining unknown in this field. As the TRPL intensity $I(\Delta t)$ at any defect emission wavelength contains contributions from both free and localized (bound) excitons, we implement a bi-exponential rise and decay model to gain insight into the lifetimes of bound and free excitons as

$$I(\Delta t) - I_{bkgd} = \sum_{j=\text{fast, slow}} \sum_{i=-\infty}^{\infty} I_{0,j} \left[\left(e^{+(\Delta t - iT)/\tau_{\text{rise},j}} \right)^{-1} + \left(e^{-(\Delta t - iT)/\tau_{\text{decay},j}} \right)^{-1} \right]^{-1}, \quad (3)$$

where I_{bkgd} is the background count rate, the subscript j indicates the fast and slow processes which we attribute to free and localized excitons respectively, the subscript i is the peak index, $I_{0,j}$ is the exciton emission intensity, Δt is the time delay, T is the period, and $\tau_{\text{rise},j}$ and $\tau_{\text{decay},j}$ are the characteristic lifetimes of excitonic rise and decay respectively. To minimize the number of adjustable parameters used in our model, all TRPL data was fit with a fully unconstrained model to obtain T=12.4415±0.0008 ns and $\tau_{\text{rise,fast}}=\tau_{\text{rise,slow}}$=7.95±0.71 ps. As the obtained period uncertainty and rise time are well below the detection limit of the silicon avalanche photodiode used in the time resolved measurements, we do not ascribe physical significance to these quantities

only to state that T and τ_{rise} are sufficiently consistent between measurements as to hold these parameters fixed at the listed values during data analysis. Subsequently the model was constrained to allow only $I_{0,j}$ and $\tau_{\text{decay},j}$ as adjustable parameters. I_{bkgd} was dark count limited at ~80-100 counts·s^{-1} which was more than 50 times below the TRPL count rate. Subsequently the model was constrained to allow only fast and slow components of $I_{0,j}$ and $\tau_{\text{decay},j}$ as adjustable parameters. Power dependence of the emission $I_{0,j}$ can be analyzed using a saturation model

$$I_{0,j}(P) = I_{0,j}(P{=}\infty) \; \frac{P}{P + P_{\text{half-sat},j}}, \tag{4}$$

where P is the excitation power, $I_{0,j}(P{=}\infty)$ is the saturation intensity, $P_{\text{half-sat}}$ is the half-saturation power, and j = fast, slow relaxation processes. Figure 2(b) demonstrates that excitation power dependences of the deconvolved emission intensities exhibit (i) a nearly linear trend for the delocalized transition (free exciton) with $I_{\infty,\text{fast}}$ = 16.4±20.0 events·s^{-1} and $P_{\text{half-sat,fast}}$ = 32.1±44.9 µW (large uncertainty is indicative of linear dependence on the excitation power) and (ii) emitters located on the top of the ultra-sharp tips (bound exciton) exhibit saturation behavior with $I_{\infty,\text{slow}}$ = 5.89±0.71 events·s^{-1} and $P_{\text{half-sat,slow}}$ = 5.36±1.16 µW. Although the emission intensity for the localized emitter is not fully saturated at the maximum power used in this study, we find that at higher powers defect emission from the sharp tips can spontaneously quench and hence we limit excitation to the low power regime in this study.

Figure 2(c) demonstrates quantum emission of a defect emission site at the apex of an ultra-sharp SiO2 tip at ~3.8K through time-dependent photon field intensity correlation, $g^{(2)}(\Delta t)$. The data can be modeled using a single exponential decay (two level) photon antibunching model[22]:

$$g^{(2)}(\Delta t) = 1 - [1 - g^{(2)}(\Delta t{=}0)] \cdot e^{-|\Delta t|/\tau_{\text{decay}}}, \tag{5}$$

where Δt is the time delay, τ_{decay} is the lifetime, $g^{(2)}(\Delta t=0)$ is the second order photon correlation parameter for single photon emission, and $[1 - g^{(2)}(\Delta t=0)]$ is defined as the single photon purity. A high degree of photon antibunching was obtained, $g^{(2)}(\Delta t=0) < 0.3$ over collection time of 45 min, and exhibited stable emission up to 8 hours. The $g^{(2)}$ spectra is normalized at far from zero (240.32 ns $\leq \Delta t \leq$ 2097.44 ns). Stability in emission intensity allowed us to obtain the intrinsic $g^{(2)}(\Delta t=0) = 0.284\pm0.062$ and an intrinsic $\tau_{\text{decay}} = 9.01\pm1.56$ ns from collections over three different times from 45 min to 8 h. We note that although the obtained τ_{decay} is in agreement with that obtained by TRPL, HBT measurements of lifetime are heavily influenced by the excitation power used in the measurement[18] making TRPL the appropriate technique for lifetime determination.

By comparing TRPL of WSe$_2$ defect emission on the tips with a WSe$_2$ defect on the substrate, we were able to decouple the intrinsic defects in the material from defects arising through engineered morphology which may elucidate the characteristics of strain-induced emission (Figure 3(a,b) and Figure S5, supplementary material). In comparison with engineered emitters where $I_{0,\text{slow}} > I_{0,\text{fast}}$, the intrinsic localized emission site we located on the substrate exhibited a slow-component emission intensity 2.9 times lower than that of the fast component, indicating dominance of the PL by the free exciton for this intrinsic defect. TRPL also revealed that the decay time for localized excitons at the apex of three representative sharp tips was 12.75, 19.47, and 68 times longer than for the free exciton, with $\tau_{\text{decay,slow}} = 11.203\pm0.660$, 15.58 ± 0.50, and 56.40 ± 7.71 ns and $\tau_{\text{decay,fast}} = 0.800\pm0.040$, 0.828 ± 0.059, and 0.879 ± 0.047 ns for the emitters shown in Figures 2(a) and 3(b). This is in comparison to the case for localized defect emission from WSe$_2$ on the substrate for which $\tau_{\text{decay,slow}}$ (2.36$\pm$0.24 ns) was only 4.8 times longer than $\tau_{\text{decay,fast}}$ (0.516$\pm$0.029 ns). The slower relaxation times for both the free and localized excitons on the tips may also be

due to phonon-mediated dark state recombination – as recently modeled for Se_W antisite defects[18] – or changes in density of states and optical phonon energies – where phonon softening may proportionately increase the lifetime[38] – although understanding the exact mechanism requires rigorous experimental and theoretical treatment in future works. The time window used in our experiment was on the order of 12.5 ns for TRPL, which was limited by the repetition rate of the laser. This explains why the longest decay time possessed a large error and is thus more qualitative in nature. We note that previous reports also indicate a wide range of decay times, roughly 0.5 to 225 ns (Table S1, supplementary material), and thus a major remaining challenge in this field is understanding the mechanisms responsible for this especially from the theoretical side. In an attempt to more accurately quantify defects intrinsically present in the epitaxial WSe_2 of this work, we have conducted Rutherford backscattering spectrometry (RBS). RBS analysis (Figure S5, supplementary material) allowed us to obtain the elemental atomic ratios of the material in this study. Analyzing the scattering yield ratios between W and Se, we obtained a W:Se ratio of 1:1.91±0.04 corresponding to a selenium deficiency of ~9%. This is considerably higher than the ~2.2% selenium deficiency obtained for crystallites synthesized through powder vaporization[39], which may lead to the variation in relaxation times we observe in this work. Confocal photoluminescence mapping around an ultra-sharp tip is shown in Figure 3(c,d) and indicates defect emission originates at the tip center.

Figure 4 gives the temperature dependent emission spectra of a localized defect emission site. Over the temperature range of 3.8 – 25 K, the emission energy remains relatively constant with a mean and standard deviation of 772.953 nm (1.604 eV) and 0.830 nm (0.00172 eV), respectively. This is in agreement with the power dependent peak emission wavelength we observed, 772.88±0.27 nm (1.604±0.001 eV) as shown in Figure S7, supplementary material, and the spectral

wandering demonstrated in previous reports[14, 15]. Similar to previous studies[7-11, 14-16, 20], localized emission is not observable at temperatures above 25 K. Figure 4(b) shows that the temperature dependent emission intensity diminishes exponentially and can be modeled as $I(T) = I_1 \cdot \exp[-T/T_c]$, with a characteristic temperature of $T_c = 5.98 \pm 0.24$ K (corresponding to a $k_B T$ energy of 515 μeV, where k_B is the Boltzmann constant). This is in agreement with the value obtained for quantum emission from monolayer WSe_2 (~300 μeV)[11]. Additionally, we observe the full width at half maximum increases exponentially from 1.42 nm (2.94 meV) at 3.8 K to 2.48 nm (5.15 meV) at 25 K and can be modeled as $\Gamma(T) = \Gamma_0 + \Gamma_1 \cdot \exp[-T/T_c]$, with a characteristic temperature of $T_c = 5.4 \pm 0.3$ K and $\Gamma_0 = 1.41 \pm 0.01$ nm (2.91 $\pm$ 0.03 meV). We note that increasing the defect trapping energy so that room temperature operation can be demonstrated may require the use of chemical-functionalization or solitary dopants as has recently been demonstrated for carbon nanotubes[25, 40], along with novel optical engineering approaches[17].

In conclusion, we have demonstrated a route to deterministically create spatially localized defect emission sites in the 750–800 nm regime using few-layer epitaxial WSe_2 and ultra-sharp SiO_2 tips, where detailed analysis of a characteristic tip proved single photon generation with $g^{(2)}(\Delta t=0) = 0.284 \pm 0.062$. Exciton lifetime increases from ~1-2 ns for a defect lying in the planar WSe_2 to ~10 ns when the defect is located on a tip apex; although this is still too small to be relevant for quantum memory applications, it is an advance in the right direction. Engineering of quantum emission in 2D materials is still in a very early stage, and further efforts are required to increase both the yield of quantum emitters and the thermal de-trapping energy for higher temperature and brighter operation. Future large-scale statistical investigations are also required to better understand defect emission including dark state, fine structure, and polarization characteristics in the 2D material/ultra-sharp tip array system. As the atomic structure of defects

responsible for localized emission is not observable in this or prior works, sustained in-depth investigations of quantum emission in 2D materials are required both from the experimental and theoretical communities.

Supplementary Material

See supplementary materials for additional comparison with existing literature, materials, methods, defect spectroscopy, and RBS results.

Acknowledgments

15RYCOR159 (J.R.H., C.K.D.). The project was conceived and led by M.T.P., and written by

M.T.P. with the assistance of W.W., C.K.D., J.R.H., and contributions from all co-authors.

References

[1]   B. Lounis and M. Orrit, Rep. Prog. Phys. **68**, 1129 (2005). http://dx.doi.org/10.1088/0034-4885/68/5/R04

[2]   C. Santori, D. Fattal, and Y. Yamamoto, *Single Photon Devices and Applications* (Wiley Verlag GmbH & Co. KGaA, Weinheim, 2010). http://www.wiley.com/WileyCDA/WileyTitle/productCd-352740807X.html

[3]   I. Aharonovich, S. Castelletto, D. A. Simpson, C. H. Su, A. D. Greentree, and S. Prawer, Rep. Prog. Phys. **74**, 076501 (2011). http://dx.doi.org/10.1088/0034-4885/74/7/076501

[4]   V. Acosta and P. Hemmer, MRS Bull. **38**, 127 (2013). http://dx.doi.org/10.1557/mrs.2013.18

[5]   L. Gordon, J. R. Weber, J. B. Varley, A. Janotti, D. D. Awschalom, and C. G. Van de Walle, MRS Bull. **38**, 802 (2013). http://dx.doi.org/10.1557/mrs.2013.206

[6]   I. Aharonovich and E. Neu, Adv. Opt. Mater. **2**, 911 (2014). http://dx.doi.org/10.1002/adom.201400189

[7]   Y.-M. He, G. Clark, J. Schaibley, R., Y. He, M.-C. Chen, Y.-J. Wei, X. Ding, Q. Zhang, W. Yao, X. Xu, C.-Y. Lu, and J.-W. Pan, Nat. Nanotechnol. **10**, 497 (2015). http://dx.doi.org/10.1038/nnano.2015.75

[8]   M. Koperski, K. Nogajewski, A. Arora, V. Cherkez, P. Mallet, J. Y. Veuillen, J. Marcus, P. Kossacki, and M. Potemski, Nat. Nanotechnol. **10**, 503 (2015). http://dx.doi.org/10.1038/nnano.2015.67

[9]   A. Srivastava, M. Sidler, A. V. Allain, D. S. Lembke, A. Kis, and A. Imamoğlu, Nat. Nanotechnol. **10**, 491 (2015). http://dx.doi.org/10.1038/nnano.2015.60

[10] P. Tonndorf, R. Schmidt, R. Schneider, J. Kern, M. Buscema, G. A. Steele, A. Castellanos-Gomez, H. S. J. van der Zant, S. Michaelis de Vasconcellos, and R. Bratschitsch, Optica **2**, 347 (2015). http://dx.doi.org/10.1364/OPTICA.2.000347

[11] C. Chakraborty, L. Kinnischtzke, K. M. Goodfellow, R. Beams, and A. N. Vamivakas, Nat. Nanotechnol. **10**, 507 (2015). http://dx.doi.org/10.1038/nnano.2015.79

[12] S. Kumar, A. Kaczmarczyk, and B. D. Gerardot, Nano Lett. **15**, 7567 (2015). http://dx.doi.org/10.1021/acs.nanolett.5b03312

[13] J. Kern, I. Niehues, P. Tonndorf, R. Schmidt, D. Wigger, R. Schneider, T. Stiehm, S. Michaelis de Vasconcellos, E. Reiter Doris, T. Kuhn, and R. Bratschitsch, Adv. Mater. **28**, 7101 (2016). http://dx.doi.org/10.1002/adma.201600560

[14] C. Palacios-Berraquero, M. Barbone, D. M. Kara, X. Chen, I. Goykhman, D. Yoon, A. K. Ott, J. Beitner, K. Watanabe, T. Taniguchi, A. C. Ferrari, and M. Atatüre, Nat. Commun. **7**, 12978 (2016). http://dx.doi.org/10.1038/ncomms12978

[15] C. Palacios-Berraquero, D. M. Kara, A. R. P. Montblanch, M. Barbone, P. Latawiec, D. Yoon, A. K. Ott, M. Loncar, A. C. Ferrari, and M. Atatüre, Nat. Commun. **8**, 15093 (2017). http://dx.doi.org/10.1038/ncomms15093

[16] A. Branny, S. Kumar, R. Proux, and B. D. Gerardot, Nat. Commun. **8**, 15053 (2017). http://dx.doi.org/10.1038/ncomms15053

[17] Y. Luo, G. D. Shepard, J. V. Ardelean, D. A. Rhodes, B. Kim, K. Barmak, J. C. Hone, and S. Strauf, Nat. Nanotechnol. **13**, 1137 (2018). http://dx.doi.org/10.1038/s41565-018-0275-z

[18] C. K. Dass, M. A. Khan, G. Clark, J. A. Simon, R. Gibson, S. Mou, X. Xu, M. N. Leuenberger, and J. R. Hendrickson, Adv. Quantum Technol. **Early View**, 1900022 (2019). http://dx.doi.org/10.1002/qute.201900022

[19] G. Noh, D. Choi, J.-H. Kim, D.-G. Im, Y.-H. Kim, H. Seo, and J. Lee, Nano Lett. **18**, 4710 (2018). http://dx.doi.org/10.1021/acs.nanolett.8b01030

[20] P. Tonndorf, S. Schwarz, J. Kern, I. Niehues, O. del Pozo-Zamudio, A. I. Dmitriev, A. P. Bakhtinov, D. N. Borisenko, N. N. Kolesnikov, A. I. Tartakovskii, S. M. de Vasconcellos, and R. Bratschitsch, 2D Mater. **4**, 021010 (2017). http://dx.doi.org/10.1088/2053-1583/aa525b

[21] P. Tonndorf, O. Del Pozo-Zamudio, N. Gruhler, J. Kern, R. Schmidt, A. I. Dmitriev, A. P. Bakhtinov, A. I. Tartakovskii, W. Pernice, S. Michaelis de Vasconcellos, and R. Bratschitsch, Nano Lett. **17**, 5446 (2017). http://dx.doi.org/10.1021/acs.nanolett.7b02092

[22] T. T. Tran, K. Bray, M. J. Ford, M. Toth, and I. Aharonovich, Nat. Nanotechnol. **11**, 37 (2016). http://dx.doi.org/10.1038/nnano.2015.242

[23] D. Andres-Penares, A. Cros, J. P. Martínez-Pastor, and J. F. Sánchez-Royo, Nanotechnology **28**, 175701 (2017). http://dx.doi.org/10.1088/1361-6528/aa669e

[24] D. M. Toyli, C. D. Weis, G. D. Fuchs, T. Schenkel, and D. D. Awschalom, Nano Lett. **10**, 3168 (2010). http://dx.doi.org/10.1021/nl102066q

[25] X. Ma, N. F. Hartmann, J. K. S. Baldwin, S. K. Doorn, and H. Htoon, Nat. Nanotechnol. **10**, 671 (2015). http://dx.doi.org/10.1038/nnano.2015.136

[26] M. S. Hofmann, J. Noé, A. Kneer, J. J. Crochet, and A. Högele, Nano Lett. **16**, 2958 (2016). http://dx.doi.org/10.1021/acs.nanolett.5b04901

[27] X. Zhang, T. H. Choudhury, M. Chubarov, Y. Xiang, B. Jariwala, F. Zhang, N. Alem, G.-C. Wang, J. A. Robinson, and J. M. Redwing, Nano Lett. **18**, 1049 (2018). http://dx.doi.org/10.1021/acs.nanolett.7b04521

[28] H. J. Conley, B. Wang, J. I. Ziegler, R. F. Haglund, S. T. Pantelides, and K. I. Bolotin, Nano Lett. **13**, 3626 (2013). http://dx.doi.org/10.1021/nl4014748

[29] C. R. Zhu, G. Wang, B. L. Liu, X. Marie, X. F. Qiao, X. Zhang, X. X. Wu, H. Fan, P. H. Tan, T. Amand, and B. Urbaszek, Phys. Rev. B **88**, 121301 (2013). http://dx.doi.org/10.1103/PhysRevB.88.121301

[30] A. Castellanos-Gomez, R. Roldán, E. Cappelluti, M. Buscema, F. Guinea, H. S. J. van der Zant, and G. A. Steele, Nano Lett. **13**, 5361 (2013). http://dx.doi.org/10.1021/nl402875m

[31] D. Lloyd, X. Liu, J. W. Christopher, L. Cantley, A. Wadehra, B. L. Kim, B. B. Goldberg, A. K. Swan, and J. S. Bunch, Nano Lett. **16**, 5836 (2016). http://dx.doi.org/10.1021/acs.nanolett.6b02615

[32] R. Schmidt, I. Niehues, R. Schneider, M. Drüppel, T. Deilmann, M. Rohlfing, S. Michaelis de Vasconcellos, A. Castellanos-Gomez, and R. Bratschitsch, 2D Mater. **3**, 021011 (2016). http://dx.doi.org/10.1088/2053-1583/3/2/021011

[33] W. Wu, J. Wang, P. Ercius, N. C. Wright, D. M. Leppert-Simenauer, R. A. Burke, M. Dubey, A. M. Dongare, and M. T. Pettes, Nano Lett. **18**, 2351 (2018). http://dx.doi.org/10.1021/acs.nanolett.7b05229

[34] W. Wong-Ng, H. F. McMurdie, B. Paretzkin, Y. Zhang, K. L. Davis, C. R. Hubbard, A. L. Dragoo, and J. M. Stewart, Powder Diffr. **2**, 257 (1987). http://dx.doi.org/10.1017/S0885715600012926

[35] I. Niehues, R. Schmidt, M. Drüppel, P. Marauhn, D. Christiansen, M. Selig, G. Berghäuser, D. Wigger, R. Schneider, L. Braasch, R. Koch, A. Castellanos-Gomez, T. Kuhn, A. Knorr, E. Malic, M. Rohlfing, S. Michaelis de Vasconcellos, and R. Bratschitsch, Nano Lett. **18**, 1751 (2018). http://dx.doi.org/10.1021/acs.nanolett.7b04868

[36] X. Hu, P. Yasaei, J. Jokisaari, S. Öğüt, A. Salehi-Khojin, and R. F. Klie, Phys. Rev. Lett. **120**, 055902 (2018). http://dx.doi.org/10.1103/PhysRevLett.120.055902

[37] P. Harris and L. Avrami, *Technical Report 4423: Some Physics of the Gruneisen Parameter* (U. S. Army Picatinney Arsenal, Dover, New Jersey, 1972), p. 39. http://www.dtic.mil/dtic/tr/fulltext/u2/751130.pdf

[38] R. Fivaz and E. Mooser, Phys. Rev. **136**, A833 (1964). http://dx.doi.org/10.1103/PhysRev.136.A833

[39] W. Wu, M. D. Morales-Acosta, Y. Wang, and M. T. Pettes, Nano Lett. **19**, 1527 (2019). http://dx.doi.org/10.1021/acs.nanolett.8b04269

[40] X. He, N. F. Hartmann, X. Ma, Y. Kim, R. Ihly, J. L. Blackburn, W. Gao, J. Kono, Y. Yomogida, A. Hirano, T. Tanaka, H. Kataura, H. Htoon, and S. K. Doorn, Nat. Photonics **11**, 577 (2017). http://dx.doi.org/10.1038/nphoton.2017.119

Figures, and Captions.
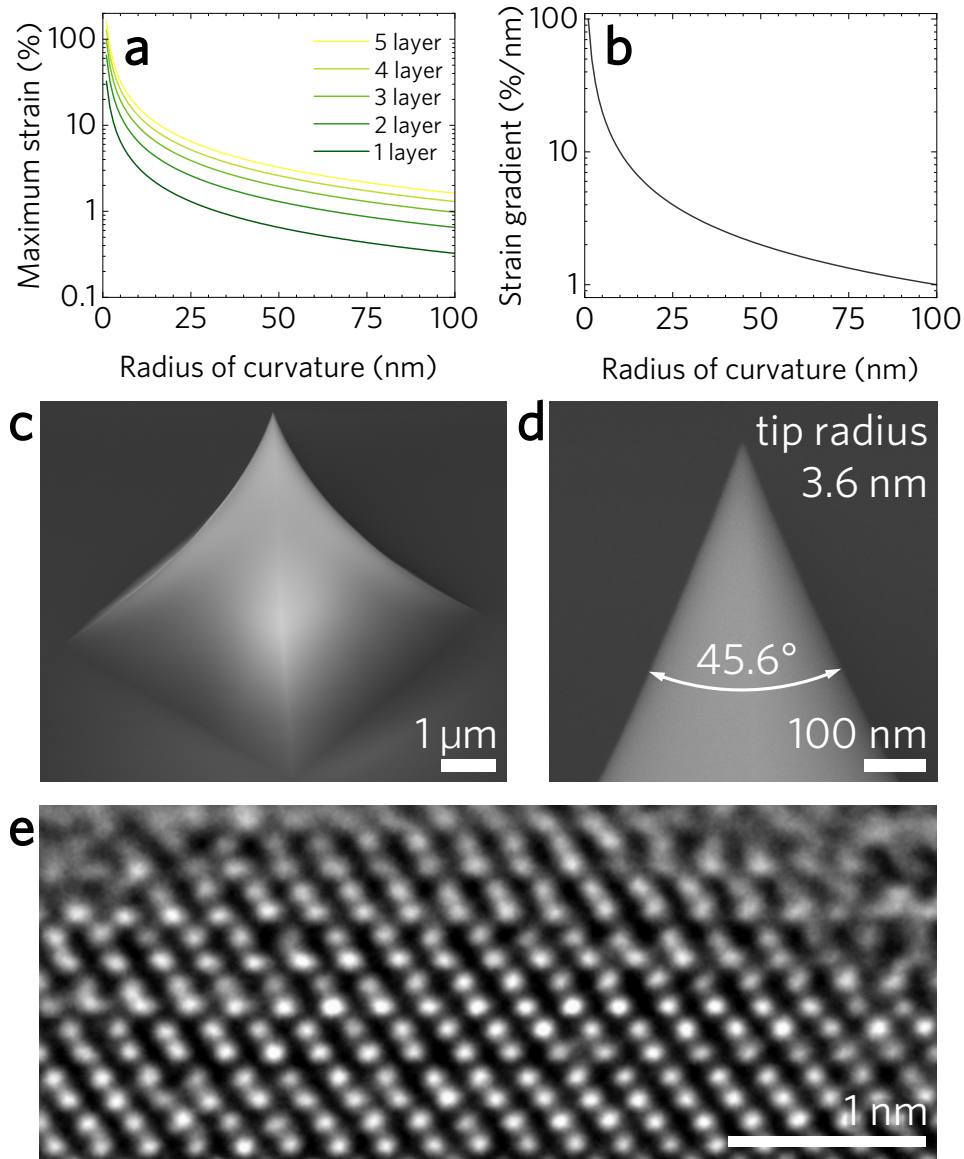
Fig. 1. Ultra-large strain and strain gradients are possible for atomically thin crystals transferred onto ultra-sharp tips. (a) Calculated maximum strain and (b) perpendicular strain gradient that will arise on the top (tensile) and bottom (compressive) surfaces of an *n*-layer WSe_2 film as a function of tip radius according to equation 1. (c-d) Scanning electron micrographs of a representative sharp tip. (e) Detail of cross-sectional transmission electron microscopy analysis illustrating a 5–10-layer thickness for the epitaxial WSe_2 in this work.
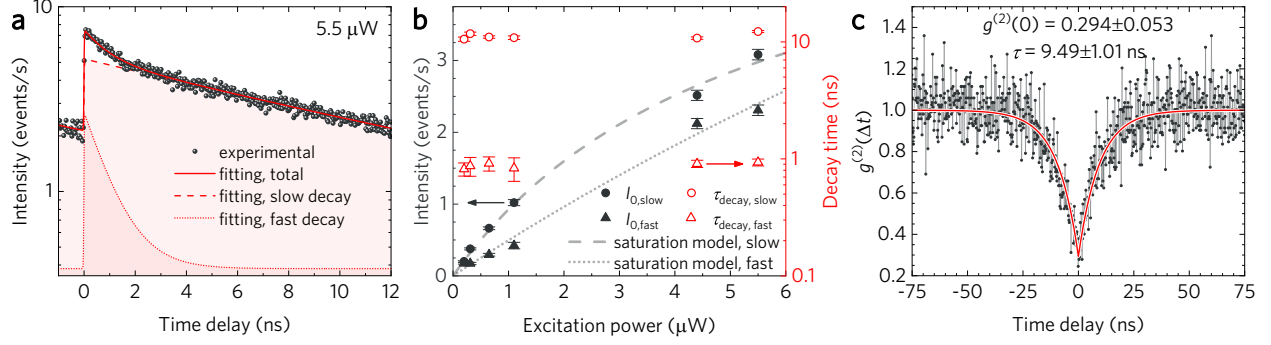
Fig. 2. Time resolved photoluminescence (TRPL) and photon field intensity correlation demonstrate spatially localized quantum emission at the apex of an ultra-sharp SiO₂ tip. (a) TRPL spectra of localized emission from WSe_2 on an ultra-sharp SiO_2 tip obtained using femtosecond excitation at 540 nm and 5.5 µW. Equation 3 is used to deconvolve bound (slow decay, dashed line) and free (fast decay, dotted line) exciton contributions to the measured event count. (b) Bound (slow decay, circles) and free (fast decay, triangles) exciton intensities (I_0, black) and decay times (τ_{decay}, red) obtained from TRPL modeled by equation 3, where error bars are defined by the 99% confidence intervals. Intensity was characterized using a saturation model given by equation 4 (slow decay, dashed line and fast decay, dotted line). (c) Measured second order photon correlation $g^{(2)}(\Delta t)$ as a function of time delay Δt and modeled according to equation 5.
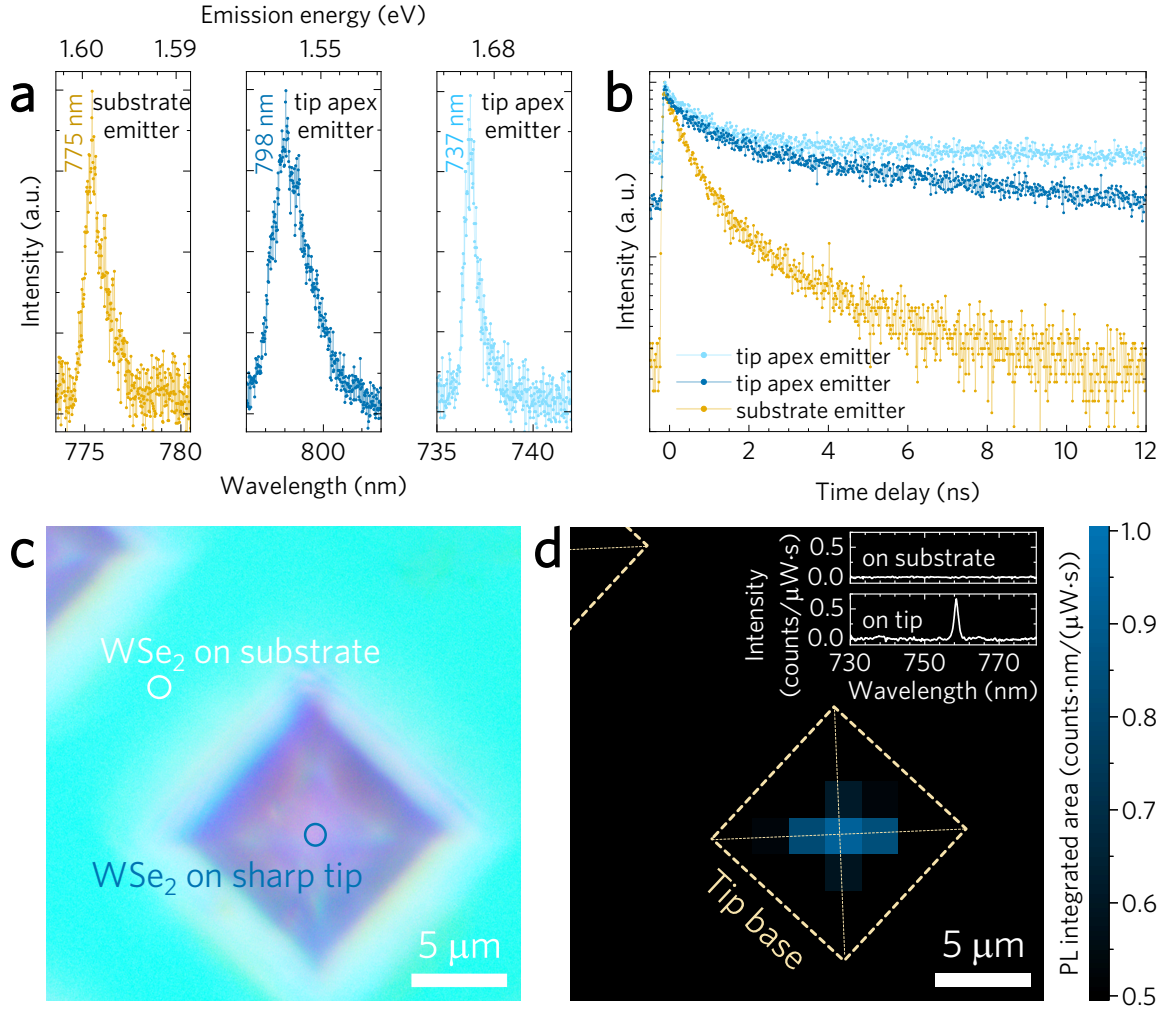
Fig. 3. Photoluminescence (PL) reveals inherent differences between 'intrinsic' and 'engineered' emission sites. (a) High resolution pulsed excitation PL of defect emission in WSe2 occurring intrinsically in the material (tan) and at the apex of ultra-sharp SiO_2 tips (blue, light blue). (b) TRPL of intrinsic [tan, corresponding to the left panel in (a)] and strain-engineered emitters [blue, corresponding to the center panel in (a), light blue corresponding to right panel in (a)]. Control over the spatial positioning of localized emission sites is demonstrated through the (c) optical micrograph and (d) scanning continuous-wave excitation PL of epitaxial WSe2 transferred onto an ultra-sharp SiO_2 tip, where the integrated area of the localized exciton peak is shown versus *x-y* coordinate.
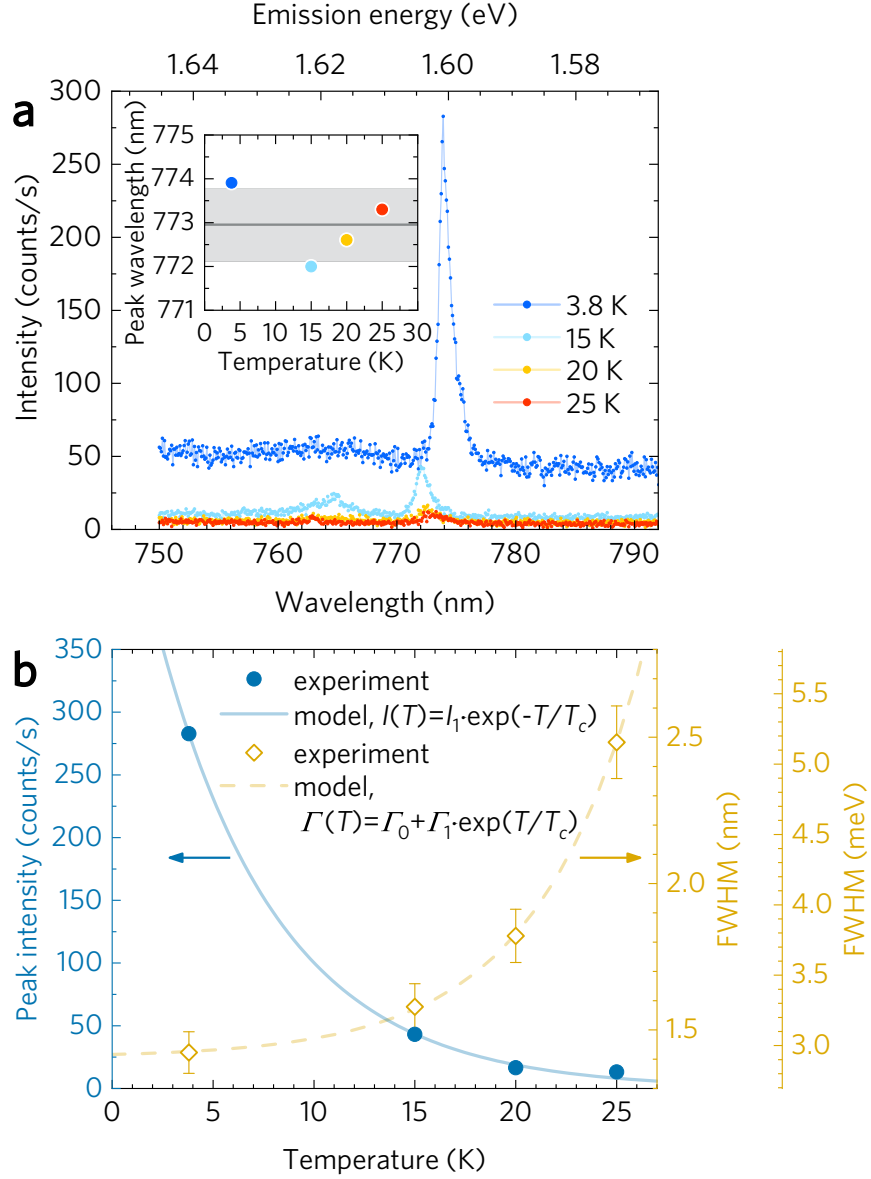
Fig. 4. Temperature dependent characteristics of localized emission. (a) Pulsed excitation PL spectra of localized emission from WSe_2 on an ultra-sharp SiO_2 tip as a function of temperature. (a, inset) Peak emission wavelength over the measured temperature range exhibits a mean of 772.95 nm and a standard deviation of 0.83 nm. (b) Peak emission intensity, I, and full width at half maximum (FWHM), Γ, versus temperature of the localized emitter. I and Γ can be modeled by exponential decay and growth models, respectively.

Locally Defined Quantum Emission from Epitaxial Few-Layer Tungsten Diselenide

Authors

Wei Wu,[1] Chandriker K. Dass,[2,3] Joshua R. Hendrickson,[2] Raul D. Montaño,[1,4] Robert E. Fischer,[5] Xiaotian Zhang,[6] Tanushree H. Choudhury,[6] Joan M. Redwing,[6,7] Yongqiang Wang,[8,9] and Michael T. Pettes[1,9,a]

Affiliations

[1] Department of Mechanical Engineering and Institute of Materials Science, University of Connecticut, Storrs, Connecticut 06269, USA.

[2] Air Force Research Laboratory, Sensors Directorate, Wright-Patterson Air Force Base, Ohio 45433, USA.

[3] KBRwyle, Dayton, OH, 45431, USA

[4] Department of Aerospace and Mechanical Engineering, University of Arizona, Tucson, Arizona 85721, USA.

[5] Center for Advanced Materials Characterization in Oregon (CAMCOR), University of Oregon, Eugene, Oregon 97403, USA.

[6] Department of Materials Science and Engineering, The Pennsylvania State University, University Park, Pennsylvania 16802, USA.

[7] 2D Crystal Consortium–Materials Innovation Platform, Materials Research Institute, The Pennsylvania State University, University Park, Pennsylvania 16802, USA.

[8] Materials Science and Technology Division, Los Alamos National Laboratory, Los Alamos, New Mexico 87545, United States

[9] Center for Integrated Nanotechnologies, Materials Physics and Applications Division, Los Alamos National Laboratory, Los Alamos, New Mexico 87545, USA.

[a] Corresponding author. Email: pettesmt@lanl.gov

Table S1. Comparison of single photon emission sources in atomically thin materials (E, λ, and τ denote the localized emission energy, wavelength, and lifetime respectively, "FSSE" denotes the fine structure splitting energy, and T denotes the temperature at which the observations were made).

| Materials	E (eV)	λ (nm)	τ (ns)	$g^{(2)}(0)$	FSSE (meV)	T (K)
WSe$_2$ (monolayer)	~1.63[1]	~760[1]	6.6-12.2[1]	0.29[1]	-	10[1]
	1.55[2]	800[2]	2.8[2]	0.07[2]	0.7-0.9[2]	3.5[2]
	1.59-1.66[3]	748-780[3]	3.1-8.8[3]	0.09-0.18[3]	0.2-0.7[3]	10[3]
	1.71[4]	726[4]	1.8-6.5[4]	0.32[4]	-	10[4]
	1.68[4]	738[4]	7.0-9.6[4]	0.28[4]	-	10[4]
	~1.69[5]	736[5]	1.5[5]	0.20[5]	-	4.2[5]
	~1.71[5]	724[5]	2.5[5]	0.18[5]	-	4.2[5]
	1.64[6]	758[6]	0.6[6]	0.3[6]	-	4.2[6]
	1.65-1.7[7]	729-751[7]	0.5-1.8[7]	0.36[7]	0.7[7]	4.2[7]
	1.58[8]	783[8]	4.14[8]	0.17[8]	0.7[8]	4[8]
	1.60-1.73[9]	719-775[9]	1.9-2.8[9]	0.19-0.23[9]	-	10[9]
	1.72[10]	721[10]	1.79[10]	0.21[10]	0.6-0.8[10]	4[10]
	1.67[11]	741[11]	2-225[11]	0.13[11]	0.45[11]	4[11]
WSe$_2$ (bilayer)	1.48-1.60[2]	775-835[2]	4.8[2]	0.03[2]	-	3.5[2]
WSe$_2$ (this work, multilayer epitaxial)	1.53-1.68	737-809	2.4 (off tip) 11-56 (on tip)	0.284	-	3.8
WS$_2$ (monolayer)	~1.93[1]	642[1]	1.4[1]	0.31[1]	-	10[1]
	1.97-2.00[3]	618-630[3]	-	-	0.3-0.8[3]	10[3]
h-BN (monolayer)	1.99[12]	623[12]	-	~0.3[12]	-	77-300[12]
h-BN (multilayer)	1.99[12]	623[12]	3.09[12]	0.33[12]	-	77-300[12]
	1.88[13]	659[13]	-	0.3-0.39[13]	-	10-300[13]
GaSe (multilayer)	1.88[14]	659[14]	-	0.33[14]	-	10[14]
	1.98-1.99[15]	623-626[15]	1[15]	0.13-0.37[15]	-	10[15]

1. Materials and Methods

1.1 CVD growth of few-layer epitaxial WSe$_2$: Reproducibility issues in the synthesis of 2D materials is a major roadblock to future large-scale device integration. In contrast to powder vaporization[16-19], chemical vapor deposition-based techniques using gaseous sources offer accessibility for future wafer scale integration, but a challenge in this growth is that the transition metal precursors have a much lower vapor pressure compared to the chalcogen precursors. This requires a much higher chalcogen concentration to form stoichiometric TMDs. A second challenge is incorporation of contaminants like carbon on the substrate from the methyl groups present in an organo-selenium precursor like dimethyl selenide[20]. In this work, we make use of a recently developed vertical cold-wall CVD reaction scheme[21] to deposit WSe$_2$ over a roughly 1 cm^2 sapphire *c*-plane (0001) substrate, where these challenges have been solved by using H$_2$Se as the selenium precursor with a significant amount of excess chalcogen – Se:W ratio of ~26,000:1 – to obtain stoichiometric and uniform films verified by x-ray photoelectron spectroscopy (Figure S1).

Tungsten diselenide films were synthesized using tungsten hexacarbonyl [W(CO)$_6$, Sigma-Aldrich, 99.99% purity] and hydrogen selenide (H$_2$Se, Matheson, 99.998% purity) in a cold-wall vertical reactor with an inductively heated SiC-coated graphite susceptor. Ultra-high purity hydrogen was used as the carrier gas through the bubblers and reactor to maintain a total flow rate at 450 sccm and a reactor pressure at 700 Torr. As-received *c*-plane (001) double-side polished sapphire (Cryscore Optoelectronic Ltd, 99.996% purity, R_a roughness < 0.2 nm) were used as substrates. The sapphire substrates were cleaned through rinsing with acetone, 2-propanol, Nano-Strip®, and deionized water prior to drying with nitrogen. The W(CO)$_6$ powder was contained inside a stainless-steel bubbler held at 30°C and 730 Torr. Initially, hydrogen carrier gas was passed through the bubbler at a flow rate of 20 sccm which resulted in a W(CO)$_6$ flow rate of

1.2×10^{-3} sccm out of the bubbler for 3 minutes. Subsequently, hydrogen carrier gas was switched to a lower flow rate of 4.5 sccm through the bubbler which resulted in a $W(CO)_6$ flow rate of 2.8×10^{-4} sccm out of the bubbler for 45 min. The H_2Se flow rate and substrate temperature were held constantly at 7 sccm and 800°C respectively during the entire growth. The significant amount of excess chalcogen – Se:W ratio of ~26,000:1 – allowed us to obtain stoichiometric and uniform films verified by X-ray photoelectron spectroscopy (Physical Electronics VersaProbe II). Figure S1 shows characterization results of the epitaxial WSe_2.
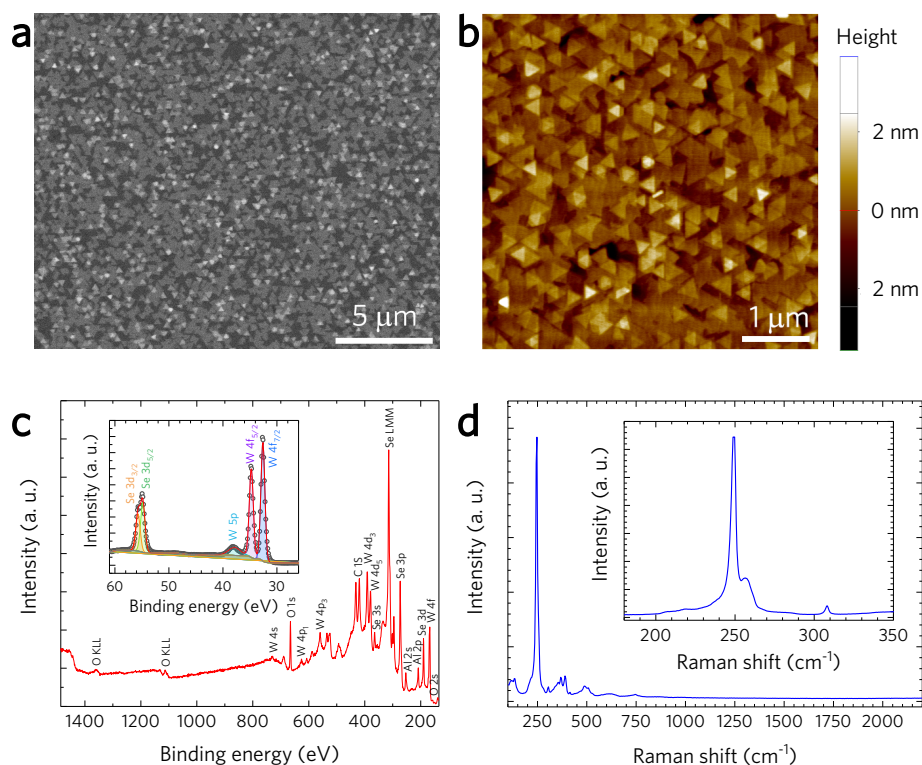
Fig. S1. Wafer-scale, few-layer epitaxial WSe_2 synthesized on *c*-plane sapphire. (a) Scanning electron micrographs (SEM) showing large-area coalesced and uniform coverage of small-grain size WSe_2 synthesized by gas source chemical vapor deposition. (b) Atomic force microscopy analysis showing textured growth of predominantly two- to three-layer WSe_2. (c) X-ray photoelectron spectroscopy analysis demonstrates a ~1:2 atomic ratio tungsten:selenium, and no detectable coordination with oxygen. (d) Raman spectroscopy exhibits no carbonaceous peaks and indicates 2–3 layer WSe_2 (inset).
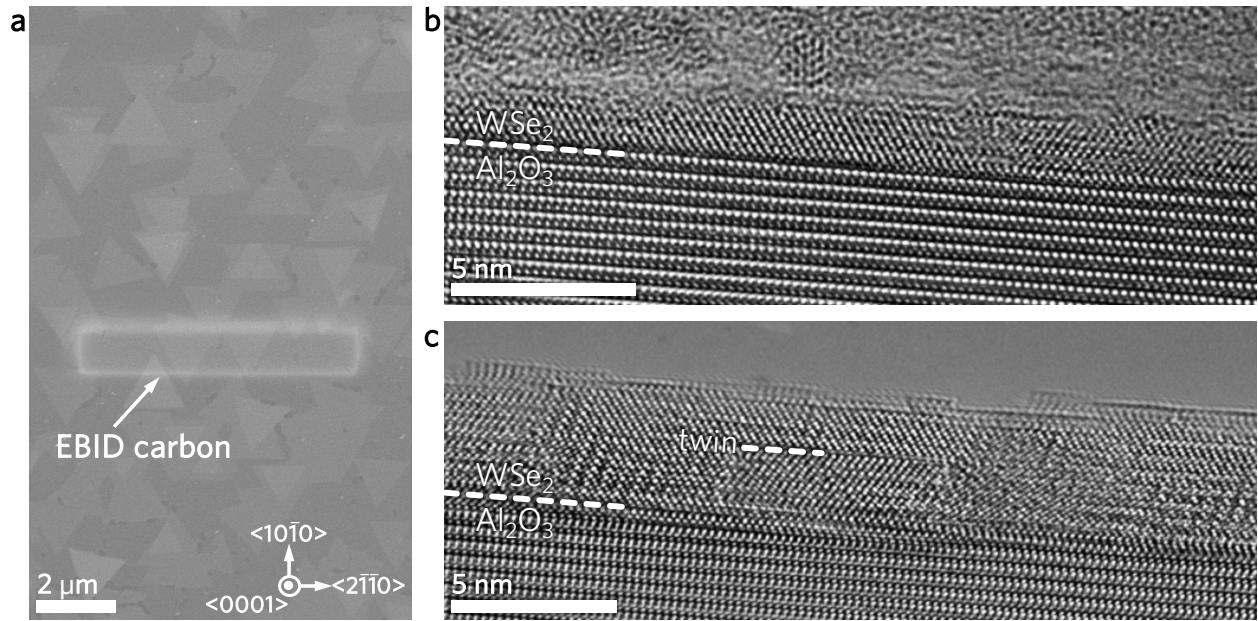
Fig. S2. Cross-sectional transmission electron microscopy (TEM) of few-layer epitaxial WSe₂ synthesized on _c_-plane sapphire. (a) SEM image showing the region subsequently patterned into a TEM foil using a focused ion beam. The surface is first protected with electron beam induced deposition (EBID) of carbon. (b-c) Phase contrast TEM images showing that twin grain boundaries are present in the material. Ultrathin cross-sections were prepared using an FEI Helios Nanolab 600i FIB-SEM. As the lamellae approached electron transparency, low energy 2 kV milling was used to avoid damaging the crystallinity of the sample. TEM was conducted using an image corrected FEI Titan 80-300 kV microscope at the LANL Electron Microscopy Laboratory operating at 300 kV. As the thickness is on the order of 5–10 layers we expect the sample should not be fully conformal to the tip (which would estimate up to 49% strain).

1.2 Transfer of few-layer epitaxial WSe₂: In contrast with previous techniques to transfer 2D materials onto flat substrates or substrates with low pattern heights[22, 23] our sharp tips tend to penetrate WSe₂, an observation also made for the dry transfer technique of ref. [3]. To overcome this, we transferred the WSe₂ by coating with PMMA and etching the sapphire substrate with KOH, then we placed the PMMA/WSe₂ film so that the PMMA was in between the WSe₂ and the SiO₂ tip acting as a buffer layer to prevent sample damage. The strain profile in this configuration

will have a complicated effect on the optical emission as it transitions from compressive to tensile across the film thickness, and it is even possible that partial puncture of the film by the tip can lead to defect emission observed in this and prior reports[2, 3], where optical emission energy would locally increase.

Transfer of the WSe_2 film from the sapphire substrate to the ultra-sharp tips was carried out by spin-coating 950,000 molecular weight PMMA (4% in anisole) onto the WSe_2/sapphire substrate at 1000 rpm for 1 minute without post baking, which resulted in a ~ 500 nm thick film. A 2.5 M potassium hydroxide (KOH) solution was used to etch the growth substrate and release the PMMA/WSe_2 composite film which was then thoroughly rinsed in deionized water. To prevent puncture, we placed the composite film so that the PMMA acted as a buffer layer between the WSe_2 and the sharp tip. We loaded the substrate into a tube furnace with 100 sccm nitrogen, purged for 2 hours, and then increased the temperature slowly from 25 to 400°C in 3 hours. The slow ramp rate softened the PMMA first to ensure contact between tip and PMMA. Thermal annealing at 400°C under nitrogen for 1 hour was then was used to remove residual PMMA and create a conformal WSe_2 film over the sharp SiO_2 tips, after which the furnace lid was opened and allowed to cool to room temperature under nitrogen flow. We note that perturbation of the electrostatic environment has been shown to give rise to photoluminescence blinking and instability[24], so that the uniform SiO_2 and residual organic complexes in our work may promote the emission intensity and spectral stability as has been shown for defect emission from aryl-group functionalized single-walled carbon nanotubes[25].

1.3 Optical measurements: The spatial PL emission and Raman spectra of WSe_2 are obtained using a confocal Raman micro-spectrometer (LabRAM HR Evolution, Horiba Scientific, Ltd.) with 2.33 eV ($\lambda = 532$ nm) continuous wave excitation at low power (86 μW) to avoid sample

damage and spectral shifts due to local heating effects. A home-built microscope-photoluminescence system was used for all pulsed excitation optical spectroscopy, TRPL, and continuous wave excitation HBT experiments. Ultrafast 540 nm excitation was provided by a Coherent Chameleon Ti:Sapphire femtosecond laser (140 fs, 80 MHz repetition rate) and Coherent VIS module. Continuous wave 543 nm excitation was provided by a Research Electro Optics R-33361 polarized helium-neon laser. The sample was placed inside of a Montana Instruments cryogen-free low-vibration cryostation with an Attocube cryogenic precision motion stage and Attocube ANC 300 piezo-controller and *in situ* 0.9 NA 100× objective. A Princeton Instruments SP2750i high performance imaging spectrograph (750 mm focal length) with a 1200 groove/mm grating [3 point resolution 0.05 nm (0.2 meV) at 543 nm] and PyLon:400BR_eXcelon back illuminated, deep depletion, liquid nitrogen-cooled CCD camera were used to collect PL spectra. TRPL and HBT measurements were conducted using a PicoQuant HydraHarp 400 multichannel picosecond event timer with TCSPC module and PicoQuant Micro Photon Devices SPD-050-CTD-FC single photon silicon avalanche photodiodes. Optical measurements involved use of Semrock tunable short- and long-pass filters, band pass filters, polarizers, and dichroic mirrors. Figure S3 illustrates the optical beam path used in this report.

In this study, we have used Semrock tunable filters in all time resolved experiments and positioned the short- and long-pass filters such that the entire defect emission peak was present in the detection path, which resulted in a band width of ~ 3 nm. As the count rate was so low, the small amount of non-quantum light that passed through the filtered region into our correlation measurements was likely the limiting factor for minimizing the $g^{(2)}(0)$ dip in our study. Since the free exciton emission will have a faster timescale and scale linearly with power, and the bound exciton emission will have a slower decay time and will show saturation behavior, we can use the

modeling shown in Figure S4 and Figure 2 of the main text to understand this behavior. We see both of these in the TRPL where the fast component showed a linear power dependence, whereas the slow component showed saturation at comparable powers. This indicated that both free and bound excitons were present in the correlation experiment as can be seen from the logarithmic intensity plot shown in Figure S5(a). The $g^{(2)}(0)$ value may possibly be improved with resonant excitation. Instead of exciting far above the band gap, which creates a large free exciton population, resonant excitation could be used to excite only the localized emitter. This would lead to reduced free exciton background and is a common technique to improve the single photon emission fidelity. Additionally, identifying emitters with energies farther away from the broad free exciton emission peak or finding emitters with brighter emission relative to the free exciton emission would also improve the single photon emission fidelity, however we note that control over the emission energies and improve the emitter brightness are still on-going efforts in the community.
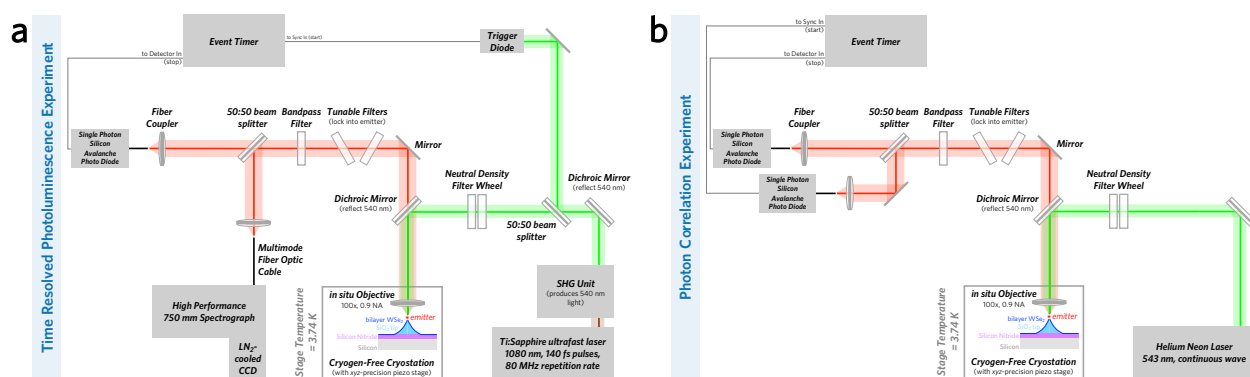
Fig. S3. Optical beam path for time resolved measurements. The excitation beam is depicted in green, and the emitter wavelength from the tip of a few-layer epitaxial WSe$_2$ sample placed on an ultra-sharp SiO$_2$ tip is depicted in red (emission is ~725-810 nm). (a) Beam path for time resolved photoluminescence (TRPL) measurements. For PL measurements, the emission beam is routed to the spectrograph. (b) Beam path for Hanbury Brown-Twiss (HBT) photon correlation measurements.
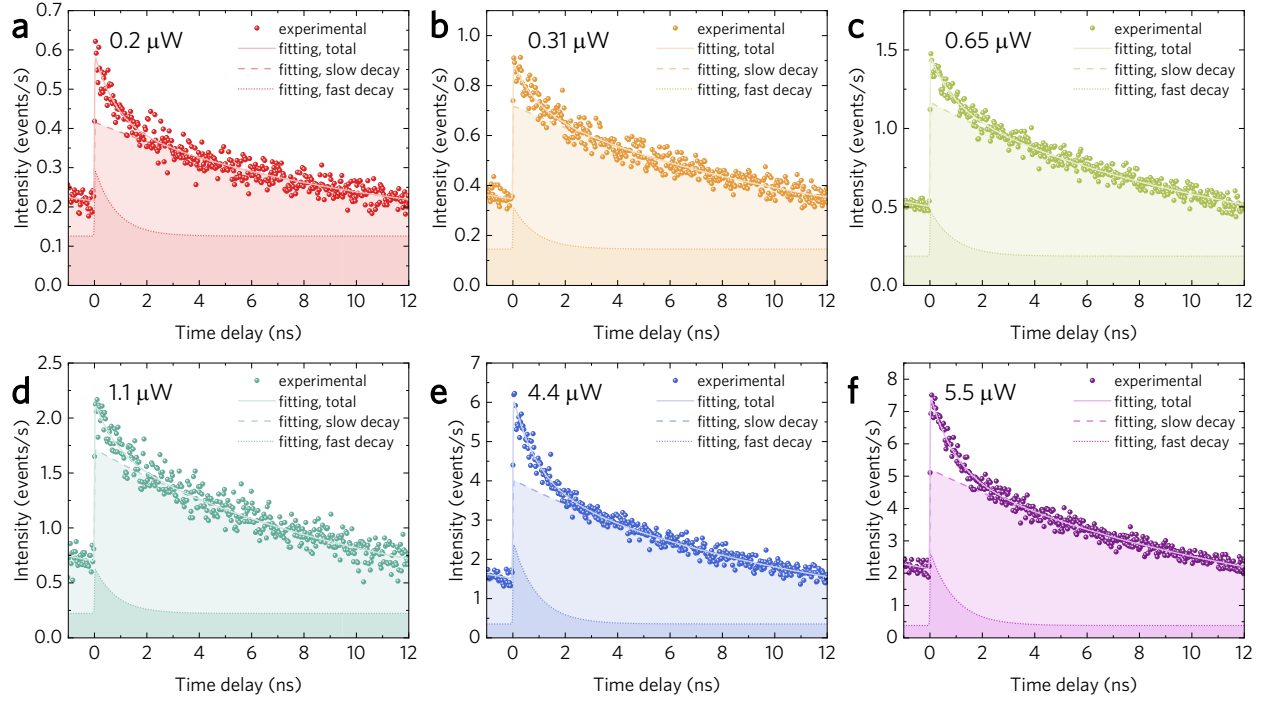
Fig. S4. Time resolved photoluminescence (TRPL) of an WSe₂ emitter at the apex of an ultra-sharp SiO₂ tip. TRPL spectra of localized emission using femtosecond excitation at 540 nm and (a) 0.20 µW, (b) 0.31 µW, (c) 0.65 µW, (d) 1.1 µW, (e) 4.4 µW, (f) 5.5 µW. Equation 3 is used to deconvolve free (fast decay, dotted line) and bound (slow decay, dashed line) exciton contributions to the measured event count.
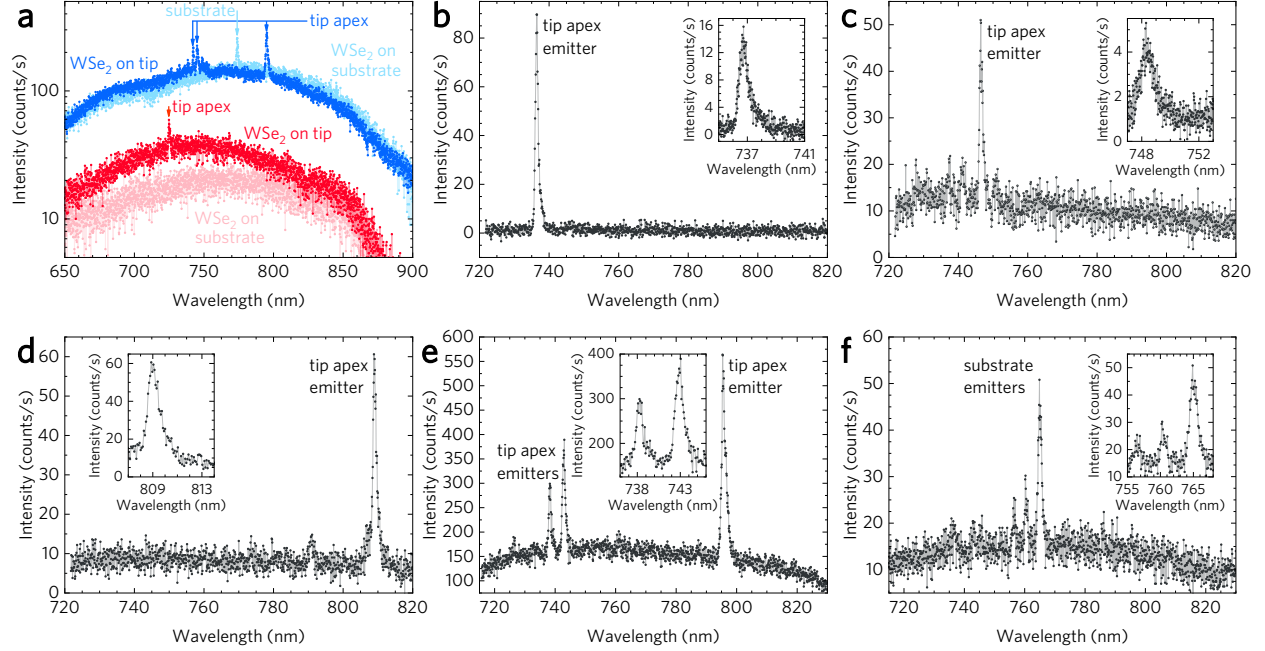
Fig. S5. Pulsed excitation photoluminescence (PL) of WSe₂. (a) Wide spectral window PL of WSe₂ at the apex of ultra-sharp SiO₂ tips (red, blue) compared with that of nearby material on the planar substrate (light red, light blue) shows a blue shift in the free exciton emission peak wavelength of $\Delta\lambda_{\text{peak}}$ = 22.1±3.4 nm (47.3±8.3 meV) and localized emission peaks. (b-e) Representative PL of emitters obtained at the center of different ultra-sharp tips and (f) obtained on the planar substrate. Free exciton emission is apparent as a broad background, giving rise to the fast decay channel obtained in the TRPL of Figure 2 in the main text and Figure S5 in the supplementary material.

2. Ion Beam Analysis
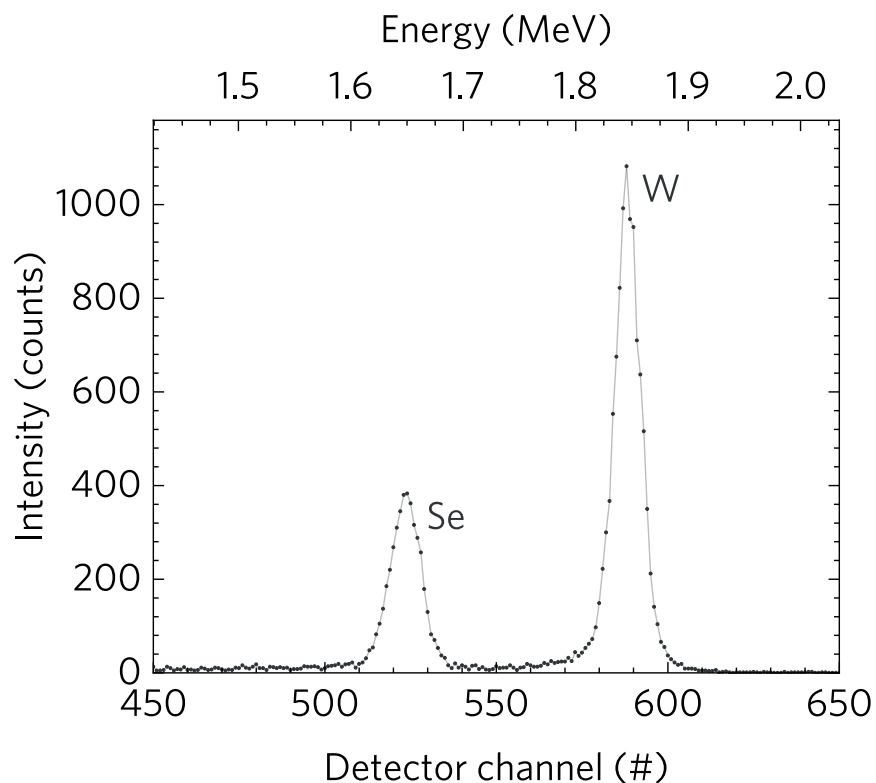
Fig. S6. Rutherford backscattering spectrometry (RBS) spectrum of epitaxial WSe$_2$. Comparison of W and Se peak areas yields stoichiometry, and background signal is sufficiently low to determine stoichiometry through the expression $c_{Se}/c_W=(A_{Se}/A_W)/(\sigma_W/\sigma_{Se})$, where c is the atomic areal density, A is the peak integrated area after background subtraction, and σ is the Rutherford scattering cross section. RBS was conducted on a National Electrostatics Corporation 3 MV Tandem Accelerator at the LANL Ion Beam Materials Laboratory using a 2 MeV ^{4}He$^+$ ion beam. A solid-state silicon detector located at 167° from the beam direction was used to detect the scattered He particles.

3. Additional Power Dependent PL and Polarization
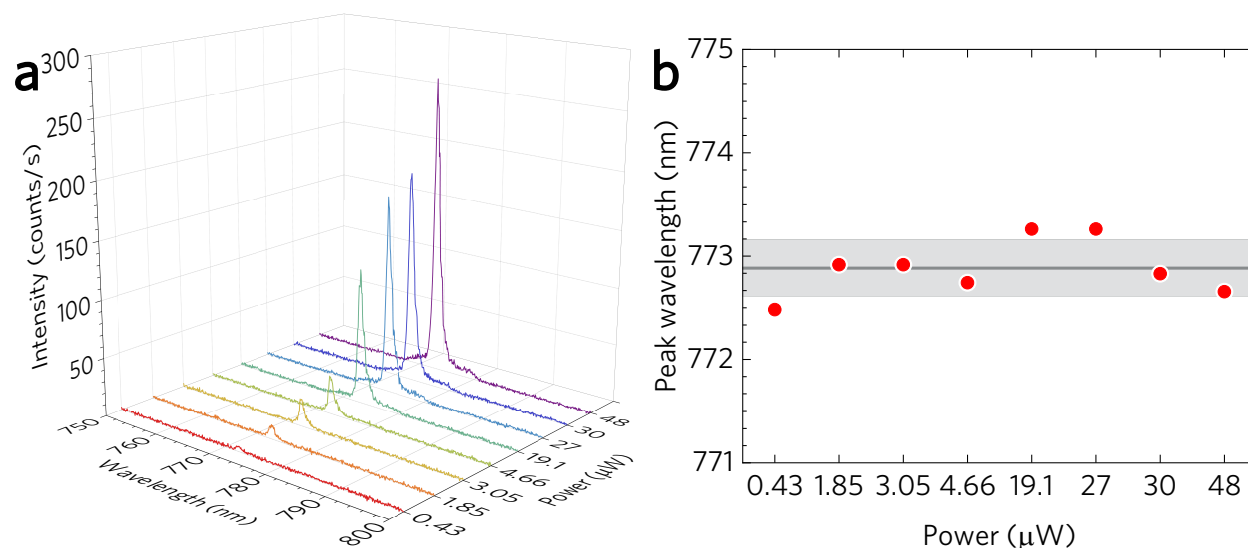
Fig. S7. Power dependence of PL. (a) PL spectra of localized emission with tunable long- and short-pass filters in place. (b) Peak emission wavelength is relatively constant over the measured excitation power range with a mean of 772.88 nm and a standard deviation of 0.27 nm.

Previous studies of defect emission in 2D materials have observed ~55–900 μeV fine structure splitting[2, 3, 5, 10, 26] and polarization[4, 8-10, 12] in the photoluminescence, both of which indicate the quantum emission thus may arise from a dipole-containing defect structure or anisotropic strain such as observed in quantum dots[27]. Within the resolution of our experimental instrumentation, ~0.05 nm (0.2 meV), we have not observed fine-structure splitting in the PL spectra of our engineered localized defects even at ~3.8 K although splitting could be hidden by the mechanisms leading to the broadened peaks we observed. Additionally, the emission is random-unpolarized when excited with linearly polarized light with a polarizer placed in the collection beam path (Figure S8, supplementary material). We note that if the emission site was actually localized because of a symmetric strain potential then there would be no preferred polarization to the emitter,

as we observed. This is unlike the case of an intrinsic defect localization, where the defect is likely to have some trap potential asymmetries. In comparison to this work, the pillars used in previous works[2, 3] are quite wide (150–280 nm diameter) with observable asymmetry, which may explain why those works observe fine structure splitting. We note that to conclusively establish mechanisms resulting in strain-based quantum emission, the atomic arrangement and induced defect structures located at the tip apex will need to be studied in more detail both through experiment and theory.
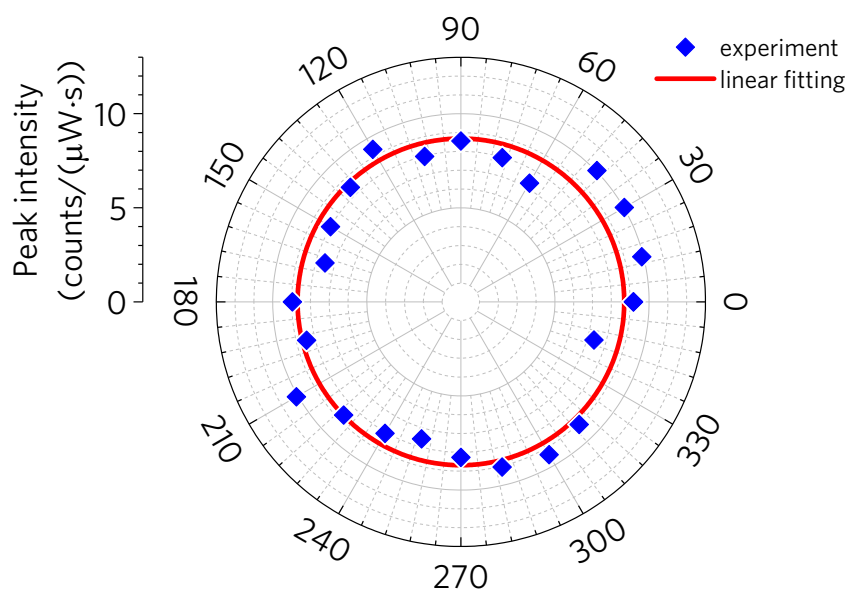
Figure S8. Polarization dependence of the localized peak emission intensity (squares) demonstrates no preferential orientation of the emitted photons, which can be fit as 8.68±0.18 counts·s^{-1}·μW^{-1} (line).

Supplementary References

[1]   C. Palacios-Berraquero, M. Barbone, D. M. Kara, X. Chen, I. Goykhman, D. Yoon, A. K. Ott, J. Beitner, K. Watanabe, T. Taniguchi, A. C. Ferrari, and M. Atatüre, Nat. Commun. **7**, 12978 (2016). http://dx.doi.org/10.1038/ncomms12978

[2]   A. Branny, S. Kumar, R. Proux, and B. D. Gerardot, Nat. Commun. **8**, 15053 (2017). http://dx.doi.org/10.1038/ncomms15053

[3]   C. Palacios-Berraquero, D. M. Kara, A. R. P. Montblanch, M. Barbone, P. Latawiec, D. Yoon, A. K. Ott, M. Loncar, A. C. Ferrari, and M. Atatüre, Nat. Commun. **8**, 15093 (2017). http://dx.doi.org/10.1038/ncomms15093

[4]   P. Tonndorf, R. Schmidt, R. Schneider, J. Kern, M. Buscema, G. A. Steele, A. Castellanos-Gomez, H. S. J. van der Zant, S. Michaelis de Vasconcellos, and R. Bratschitsch, Optica **2**, 347 (2015). http://dx.doi.org/10.1364/OPTICA.2.000347

[5]   A. Srivastava, M. Sidler, A. V. Allain, D. S. Lembke, A. Kis, and A. Imamoğlu, Nat. Nanotechnol. **10**, 491 (2015). http://dx.doi.org/10.1038/nnano.2015.60

[6]   M. Koperski, K. Nogajewski, A. Arora, V. Cherkez, P. Mallet, J. Y. Veuillen, J. Marcus, P. Kossacki, and M. Potemski, Nat. Nanotechnol. **10**, 503 (2015). http://dx.doi.org/10.1038/nnano.2015.67

[7]   C. Chakraborty, L. Kinnischtzke, K. M. Goodfellow, R. Beams, and A. N. Vamivakas, Nat. Nanotechnol. **10**, 507 (2015). http://dx.doi.org/10.1038/nnano.2015.79

[8]   S. Kumar, A. Kaczmarczyk, and B. D. Gerardot, Nano Lett. **15**, 7567 (2015). http://dx.doi.org/10.1021/acs.nanolett.5b03312

[9]   J. Kern, I. Niehues, P. Tonndorf, R. Schmidt, D. Wigger, R. Schneider, T. Stiehm, S. Michaelis de Vasconcellos, E. Reiter Doris, T. Kuhn, and R. Bratschitsch, Adv. Mater. **28**, 7101 (2016). http://dx.doi.org/10.1002/adma.201600560

[10]   Y.-M. He, G. Clark, J. Schaibley, R., Y. He, M.-C. Chen, Y.-J. Wei, X. Ding, Q. Zhang, W. Yao, X. Xu, C.-Y. Lu, and J.-W. Pan, Nat. Nanotechnol. **10**, 497 (2015). http://dx.doi.org/10.1038/nnano.2015.75

[11]   C. K. Dass, M. A. Khan, G. Clark, J. A. Simon, R. Gibson, S. Mou, X. Xu, M. N. Leuenberger, and J. R. Hendrickson, Adv. Quantum Technol. **Early View**, 1900022 (2019). http://dx.doi.org/10.1002/qute.201900022

[12]   T. T. Tran, K. Bray, M. J. Ford, M. Toth, and I. Aharonovich, Nat. Nanotechnol. **11**, 37 (2016). http://dx.doi.org/10.1038/nnano.2015.242

[13]   G. Noh, D. Choi, J.-H. Kim, D.-G. Im, Y.-H. Kim, H. Seo, and J. Lee, Nano Lett. **18**, 4710 (2018). http://dx.doi.org/10.1021/acs.nanolett.8b01030

[14]   P. Tonndorf, S. Schwarz, J. Kern, I. Niehues, O. del Pozo-Zamudio, A. I. Dmitriev, A. P. Bakhtinov, D. N. Borisenko, N. N. Kolesnikov, A. I. Tartakovskii, S. M. de Vasconcellos, and R. Bratschitsch, 2D Mater. **4**, 021010 (2017). http://dx.doi.org/10.1088/2053-1583/aa525b

[15]   P. Tonndorf, O. Del Pozo-Zamudio, N. Gruhler, J. Kern, R. Schmidt, A. I. Dmitriev, A. P. Bakhtinov, A. I. Tartakovskii, W. Pernice, S. Michaelis de Vasconcellos, and R. Bratschitsch, Nano Lett. **17**, 5446 (2017). http://dx.doi.org/10.1021/acs.nanolett.7b02092

[16]   J.-K. Huang, J. Pu, C.-L. Hsu, M.-H. Chiu, Z.-Y. Juang, Y.-H. Chang, W.-H. Chang, Y. Iwasa, T. Takenobu, and L.-J. Li, ACS Nano **8**, 923 (2014). http://dx.doi.org/10.1021/nn405719x

[17]   C. Huang, S. Wu, A. M. Sanchez, J. J. P. Peters, R. Beanland, J. S. Ross, P. Rivera, W. Yao, D. H. Cobden, and X. Xu, Nat. Mater. **13**, 1096 (2014). http://dx.doi.org/10.1038/nmat4064

[18]   H. Zhou, C. Wang, J. C. Shaw, R. Cheng, Y. Chen, X. Huang, Y. Liu, N. O. Weiss, Z. Lin, Y. Huang, and X. Duan, Nano Lett. **15**, 709 (2015). http://dx.doi.org/10.1021/nl504256y

[19]   J. Chen, B. Liu, Y. Liu, W. Tang, C. T. Nai, L. Li, J. Zheng, L. Gao, Y. Zheng, H. S. Shin, H. Y. Jeong, and K. P. Loh, Adv. Mater. **27**, 6722 (2015). http://dx.doi.org/10.1002/adma.201503446

[20]   X. Zhang, Z. Y. Al Balushi, F. Zhang, T. H. Choudhury, S. M. Eichfeld, N. Alem, T. N. Jackson, J. A. Robinson, and J. M. Redwing, J. Electron. Mater. **45**, 6273 (2016). http://dx.doi.org/10.1007/s11664-016-5033-0

[21]   X. Zhang, T. H. Choudhury, M. Chubarov, Y. Xiang, B. Jariwala, F. Zhang, N. Alem, G.-C. Wang, J. A. Robinson, and J. M. Redwing, Nano Lett. **18**, 1049 (2018). http://dx.doi.org/10.1021/acs.nanolett.7b04521

[22]   J. W. Suk, A. Kitt, C. W. Magnuson, Y. Hao, S. Ahmed, J. An, A. K. Swan, B. B. Goldberg, and R. S. Ruoff, ACS Nano **5**, 6916 (2011). http://dx.doi.org/10.1021/nn201207c

[23]   Y.-H. Lee, L. Yu, H. Wang, W. Fang, X. Ling, Y. Shi, C.-T. Lin, J.-K. Huang, M.-T. Chang, C.-S. Chang, M. Dresselhaus, T. Palacios, L.-J. Li, and J. Kong, Nano Lett. **13**, 1852 (2013). http://dx.doi.org/10.1021/nl400687n

[24]   N. F. Hartmann, S. E. Yalcin, L. Adamska, E. H. Haroz, X. Ma, S. Tretiak, H. Htoon, and S. K. Doorn, Nanoscale **7**, 20521 (2015). http://dx.doi.org/10.1039/C5NR06343D

[25]   X. He, N. F. Hartmann, X. Ma, Y. Kim, R. Ihly, J. L. Blackburn, W. Gao, J. Kono, Y. Yomogida, A. Hirano, T. Tanaka, H. Kataura, H. Htoon, and S. K. Doorn, Nat. Photonics **11**, 577 (2017). http://dx.doi.org/10.1038/nphoton.2017.119

[26]   Y. Luo, G. D. Shepard, J. V. Ardelean, D. A. Rhodes, B. Kim, K. Barmak, J. C. Hone, and S. Strauf, Nat. Nanotechnol. **13**, 1137 (2018). http://dx.doi.org/10.1038/s41565-018-0275-z

[27]   D. Gammon, E. S. Snow, B. V. Shanabrook, D. S. Katzer, and D. Park, Phys. Rev. Lett. **76**, 3005 (1996). http://dx.doi.org/10.1103/PhysRevLett.76.3005